Enhanced excitation-coupled Ca^{2+} entry induces nuclear translocation of NFAT and contributes to IL-6 release from myotubes from patients with central core disease

Susan Treves[1,2,3,*], **Mirko Vukcevic**[1,2], **Pierre-Yves Jeannet**[4], **Soledad Levano**[1,2], **Thierry Girard**[1,2], **Albert Urwyler**[1,2], **Dirk Fischer**[5,6], **Thomas Voit**[7], **Heinz Jungbluth**[8,9], **Sue Lillis**[10], **Francesco Muntoni**[11], **Ros Quinlivan**[12], **Anna Sarkozy**[13], **Kate Bushby**[13] **and Francesco Zorzato**[1,2,3,*]

[1]Department of Anesthesia and [2]Department of Biomedicine, Basel University Hospital, 4031 Basel, Switzerland, [3]Dipartimento di Medicina Sperimentale e Diagnostica, sez Patologia Generale, University of Ferrara, Ferrara, Italy, [4]Unité de Neuropédiatrie CHUV - BH11, 1011 Lausanne, Switzerland, [5]Department of Neuropediatrics, University Children's Hospital, Basel, Switzerland, [6]Department of Neurology, Basel University Hospital, 4031 Basel, Switzerland, [7]Institut de Myologie, Groupe Hospitalier Pitié-Salpêtrière, UPMC, Paris, France, [8]Department of Paediatric Neurology – Neuromuscular Service, Evelina Children's Hospital, Guy's & St Thomas' NHS Foundation Trust, London, UK, [9]Clinical Neuroscience Division IOP, King's College London, IOP, London, UK, [10]Diagnostic DNA Laboratory, GSTT Pathology, Guy's Hospital, London, UK, [11]Dubowitz Neuromuscular Centre, UCL Institute of Child Health, London, UK, [12]Wolfson Centre of Inherited Neuromuscular Disease, Robert Jones and Agnes Hunt Orthopaedic Hospital NHS Trust, Oswestry SY10 7AG, UK and [13]Institute of Human Genetics, Newcastle University, Newcastle upon Tyne, UK

Prolonged depolarization of skeletal muscle cells induces entry of extracellular calcium into muscle cells, an event referred to as excitation-coupled calcium entry. Skeletal muscle excitation-coupled calcium entry relies on the interaction between the 1,4-dihydropyridine receptor on the sarcolemma and the ryanodine receptor on the sarcoplasmic reticulum membrane. In this study, we directly measured excitation-coupled calcium entry by total internal reflection fluorescence microscopy in human skeletal muscle myotubes harbouring mutations in the *RYR1* gene linked to malignant hyperthermia (MH) and central core disease (CCD). We found that excitation-coupled calcium entry is strongly enhanced in cells from patients with CCD compared with individuals with MH and controls. Furthermore, excitation-coupled calcium entry induces generation of reactive nitrogen species and enhances nuclear localization of NFATc1, which in turn may be responsible for the increased IL-6 released by myotubes from patients with CCD.

INTRODUCTION

Excitation–contraction coupling (E–C coupling) is the process whereby an electrical signal generated at the nerve terminal is converted into a chemical signal, i.e. release of

Ca^{2+} from the sarcoplasmic reticulum (SR), leading to muscle contraction and force development (1–3). Although many proteins are involved in skeletal muscle E–C coupling, the two key players are Ca^{2+} channels: the voltage-sensing dihydropyridine receptor (DHPR), an L-type Ca^{2+} channel

---

($Ca_v1.1$) present on the transverse tubules, and the ryanodine receptor (RyR1), an intracellular Ca^{2+} release channel localized on the SR terminal cisternae (2,4,5). Dysregulation of calcium signals due to defects in RyR1 and $Ca_v1.1$ is the underlying feature of malignant hyperthermia (MH; MIM 145600), a pharmacogenetic potentially lethal reaction during anaesthesia, as well as several congenital myopathies, including central core disease (CCD) characterized by muscle weakness, fibre type-1 predominance and cores running the length of the muscle fibre (CCD; MIM 11700), subgroups of multiminicore disease (MIM 255320), certain forms of centronuclear myopathy (6) and congenital fibre-type disproportion (7). A great deal of data indicate that heterozygous *RYR1* mutations associated with the CCD phenotype result in leaky channels, leading to the depletion of Ca^{2+} from SR stores (8–11). The 'leaky channel' hypothesis has been challenged by data obtained using myotubes from RyR1 knock out animals reconstituted with recombinant RyR1 cDNA carrying the C-terminal (domain 3) *RYR1* mutations p.I4898T, p.G4890R, p.R4892W, p.G4898R, p.A4905V (12–14). Results using this model system have suggested the alternative 'E–C uncoupling' hypothesis (15). The leaky channel hypothesis predicts a decrease of the SR Ca^{2+} load, whereas the E–C uncoupling hypothesis predicts that the muscle weakness does not result from major changes in the SR Ca^{2+} levels, but rather is due to a defect in the molecular mechanism underlying the transmission of the signal from sarcolemmal depolarization to the RyR1 (reviewed in 16). The alteration of SR calcium load determined by calcium leak is associated to an increase of the resting calcium concentration in myotubes from CCD patients (8,13), and this represents a second major difference between the leaky and E–C uncoupling hypothesis. In resting conditions, the level of intracellular $[Ca^{2+}]$ is ultimately determined by the influx of Ca^{2+} from the extracellular environment which represents an 'unlimited' Ca^{2+} sink and is much larger than the Ca^{2+} present within the SR stores (17). If this were true, the leaky channel hypothesis would also predict an increase of calcium influx in muscle cells from CCD and MH susceptible (MHS) patients. Calcium influx in muscle cells is operated by two main mechanisms: excitation-coupled Ca^{2+} entry (ECCE) and store-operated Ca^{2+} entry (SOCE). ECCE requires the functional interaction between the DHPR and the RyR1 (18,19). Interestingly, dyspedic mouse myotubes over-expressing RyR1 cDNA harbouring a mutation linked to MHS display enhanced ECCE (20,21). However, experiments carried out in intact adult and fetal mammalian skeletal muscle fibres have shown that SOCE is mediated by Orai1 and Stim1 (22). It is plausible that SOCE may be physiologically involved in refilling depleted SR stores after intense muscle activity/or when the store is leaky, as in the case of CCD-linked *RYR1* mutations. Alterations of Ca^{2+} entry and elevation of the resting $[Ca^{2+}]$ may induce downstream events including (i) nuclear translocation of Ca^{2+}-sensitive transcription factors involved in fibre-type differentiation (23,24), and (ii) activation of membrane-associated calcium-dependent enzymes such as NO synthase (NOS) (25). Each of these events and/or the combination of both may be responsible, at least in part, for some of the phenotypes induced by *RYR1* mutations. In this study,

we tested the hypothesis that human myotubes carrying mutations linked to CCD and MHS display enhanced ECCE and that the calcium influx via ECCE is associated with downstream events which may be implicated in the pathophysiology of *RYR1*-related channelopathies. Our results show that cells from MHS and CCD patients exhibit a significantly higher ECCE compared with myotubes from control individuals. Enhanced ECCE is linked to the activation of NOS and to the nuclear translocation of nuclear factor of activated T cells (NFAT), and may contribute to the increased release of IL-6 from myotubes from CCD patients.

RESULTS

Ca^{2+} homeostasis in muscle cells from control, MHS and CCD patients

Figure 1 shows the resting $[Ca^{2+}]$ and peak Ca^{2+} increase induced by 100 mM KCl in myotubes from control individuals and cells from patients with MHS and CCD. The presence of the *RYR1* mutation p.V2168M in muscle cells from MHS individuals caused a small increase in the resting $[Ca^{2+}]$. In our hands, none of the other heterozygous MHS-linked mutations significantly affected the resting $[Ca^{2+}]$, whereas it was slightly but significantly elevated in all cells obtained from patients with clinically and histopathologically confirmed CCD (Fig. 1A). In addition, the peak Ca^{2+} in response to stimulation with 100 mM KCl in the presence of 100 μM La^{3+} was not different in myotubes from control and MHS-*RYR1*-mutation-bearing individuals, whereas cells from all patients with CCD showed a significant reduction in Ca^{2+} release (Fig. 1B). These results on global Ca^{2+} homeostasis are compatible with previous results by us and others on the general characteristics of cells bearing *RYR1* mutations (8,13,26,27), and confirm that, irrespective of the underlying mechanism, the peak Ca^{2+} response to KCl in myotubes from MHS and control individuals is similar, whereas cells from CCD individuals release less Ca^{2+} when depolarized.

Total internal reflection fluorescence microscopy in fluo-4-loaded control human myotubes

The increased SR calcium leak via mutated RyR1 channels has been proposed to be responsible for the transient increase of the resting $[Ca^{2+}]$. The steady increase of the resting $[Ca^{2+}]$ is ultimately due to an increased Ca^{2+} influx from the extracellular environment into the myoplasm (17). Thus, one would predict that the presence of leaky RyR1 channels which are accompanied by increases in the resting $[Ca^{2+}]$ should be linked to alterations of Ca^{2+} influx. We set out to test this hypothesis by investigating influx by exploiting total internal reflection fluorescence (TIRF) microscopy in combination with changes in the fluorescence of the fast Ca^{2+} indicator fluo-4. TIRF microscopy is the best optical technology available to monitor membrane- associated events at very high resolution (28). Figure 2 shows the application of such a technique to study Ca^{2+} influx in control human myotubes. Figure 2A shows photomicrographs of myotubes by brightfield microscopy (top left panel) and with a surface reflection
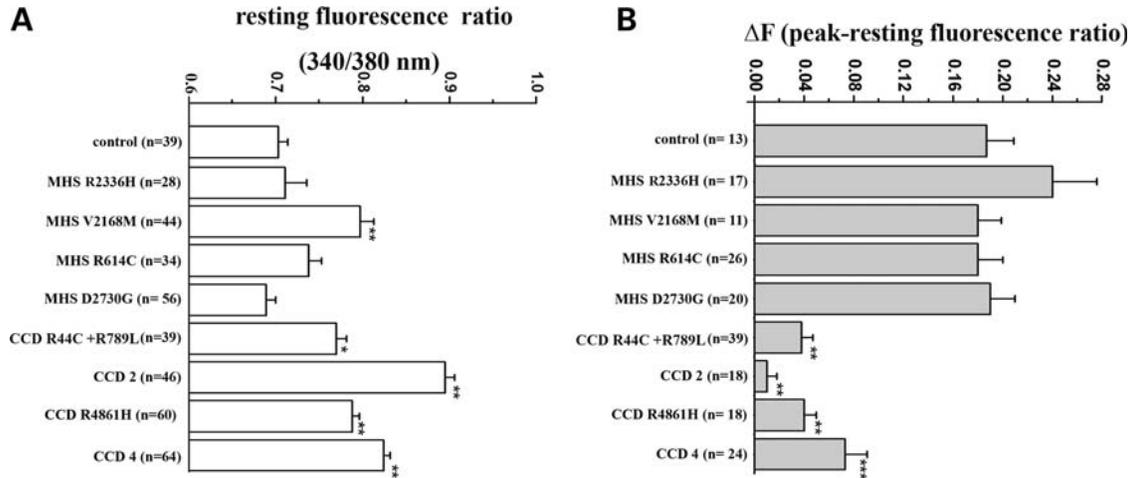
Figure 1. Cytoplasmic Ca^{2+} homeostasis in myotubes from controls, MHS and CCD patients. (**A**) Average resting myoplasmic $[Ca^{2+}]$ (fura-2 fluorescence ratio) of human myotubes from three healthy controls and from the indicated MHS and CCD patients. Measurements (mean $\pm$ SEM) were made on cells perfused in Krebs–Ringer containing 2 mM Ca^{2+}. (**B**) Mean ($\pm$ SEM) peak global $[Ca^{2+}]$ increase of myotubes to 100 mM KCl Krebs–Ringer containing 100 μM La^{3+}. Statistical analysis was performed using the ANOVA test followed by Dunnett's *post hoc* test. $^*P < 0.0004$, $^{**}P < 0.0001$, $^{***}P < 0.0015$ compared with cells from control individuals.

interference contrast (SRIC) filter (top central panel) in order to visualize the contact sites between the myotubes and the glass coverslip (dark grey area). Cells were then excited at 488 nm using a Sapphire laser to monitor fluo-4 fluorescence (top right panel), and the focal plane was fixed by means of the Perfect Focus System (PFS) at the focal plane which had been used to identify the 'footprint' of the cell on the glass coverslip. The bottom panels of Figure 2A show time-lapse changes (F/F_0) in fluo-4 fluorescence during the application of 100 mM KCl to cells which had been pre-treated with 500 μM ryanodine to block the release of Ca^{2+} from the SR stores via RyRs (29,30). Prolonged KCl depolarization results in a non-homogeneous increase of fluo-4 fluorescence within the 100 nm space adjacent to the sarcolemma. Because the localization and intensity of fluo-4 fluorescent areas detected in TIRF mode showed high variability within and between cells, we measured the average increase of fluo-4 fluorescence over the entire cell footprint (Fig. 2B and C). We believe that the increase of fluo-4 fluorescence is indicative of ECCE, since the pharmacological profile of the Ca^{2+} response closely matches that ascribed to ECCE (19); in particular: (i) it was dependent on the presence of extracellular Ca^{2+} and did not occur in cells perfused with KCl plus 100 μM La^{3+}, a non-specific blocker of plasma membrane Ca^{2+} channels; (ii) it was blocked by pre-treatment of cells with 10 μM nifedipine and by 10 μM SKF-96365, a selective inhibitor of receptor-mediated Ca^{2+} entry and voltage-gated Ca^{2+} entry (31,32) (Fig. 2B and C). These results support the use of TIRF microscopy to directly measure changes in $[Ca^{2+}]$ occurring within a domain very close to the plasma membrane.

Excitation-coupled calcium entry in myotubes from MHS and CCD patients

Having established the conditions to detect Ca^{2+} influx by TIRF microscopy, we studied ECCE in fluo-4-loaded cells

from MHS and CCD patients and compared the peak change in Ca^{2+} with that observed in myotubes from control individuals. Figure 3 shows the cumulative data obtained on ECCE in myotubes from three control individuals and from myotubes obtained from the different patients bearing the indicated *RYR1* mutations. We assessed the variability of ECCE in myotubes from controls (Supplementary Material, Fig. S1) and compared the average value with that from MHS and CCD myotubes. Under our experimental conditions, the cells from MHS patients harbouring *RYR1* mutations, except for those harbouring the p.R2336H and p.R614C substitutions, exhibited a significantly higher ECCE (ranging from $\sim$1.3–1.5 fold) compared with that observed in control cells. The most striking result was observed in cells from CCD patients, which exhibited a 1.5–2.66-fold increase in ECCE compared with that observed in control cells. To determine whether the increase in ECCE in MHS and CCD myotubes is linked to changes in the expression of the DHPR, we examined the content of the $Ca_v1.1$ transcript by real-time PCR. We found that the levels of expression of $Ca_v1.1$ were 1 ± 0.4, 0.78 ± 0.24 and 1.67 ± 0.44 in control, MHS and CCD myotubes, respectively (mean $\pm$ SD, $n = 3$). The increase, if any, of $Cav1.1$ transcript in CCD was not statistically significant ($P < 0.123$), and appears to be too low to account for the extent of ECCE increase in CCD myotubes.

We reasoned that the larger depolarization-induced Ca^{2+} influx in cells from CCD patients compared with that measured in myotubes from both controls and MHS patient may represent a mechanism underlying not only the increased resting $[Ca^{2+}]$, but also the physiological activation of membrane-bound Ca^{2+}-dependent enzymes. A previous study on a knock-in animal model carrying the Y522S MHS-associated substitution showed that myotubes from the knock-in but not from control mouse display higher reactive nitrogen species (RNS) generation, most likely due to the activation of NOS (33). On the basis of these observations on the mouse model, we examined whether alterations of ECCE might affect RNS generation via
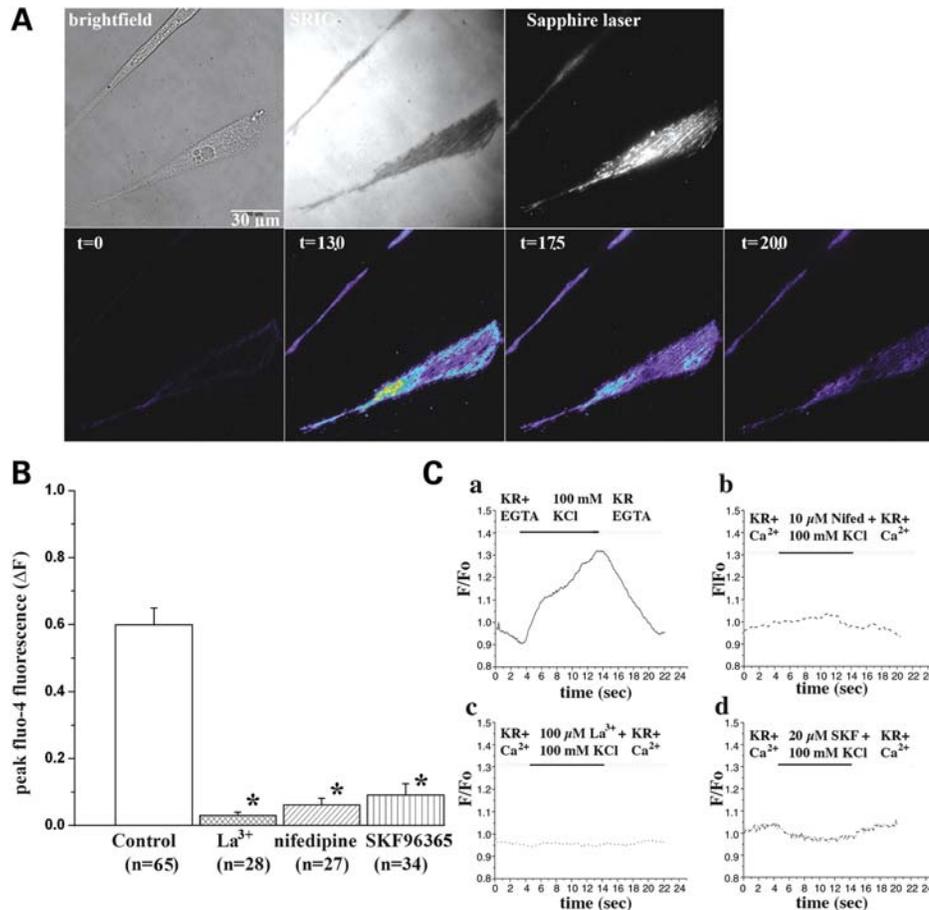
Figure 2. TIRF measurements of Ca^{2+} influx induced by KCl in human myotubes. (**A**) Myotubes from a control patient were visualized by brightfield (top left panel), with an SRIC filter to visualize and fix the focal plane of the coverglass/cell membrane interphase (top central panel) and by exciting fluo-4 with a Sapphire laser (488 excitation, top right panel) and by monitoring membrane fluorescence. The bottom panels show pseudo-coloured ratiometric images (peak fluorescence after addition of KCl/resting fluorescence) of fluo-4 fluorescence changes at the indicated time-points after application of KCl. Cells which had been pre-treated with 500 μM ryanodine during fluo-4 loading were individually stimulated with 100 mM KCl and the changes in fluorescence were monitored as detailed in Materials and Methods. Bar indicates 30 μm. Images were acquired through a $60\times$ TIRF objective and analysed using Metamorph. (**B**) Mean ($\pm$ SEM) peak increase of fluo-4 fluorescence induced by 100 mM KCl in the presence of 100 μM La^{3+}, 10 μM nifedipine and 10 μM SKF-96365. Statistical analysis was performed using the ANOVA test followed by Dunnett's *post hoc* test. $^*P < 0.0001$ compared with untreated cells. (**C**) Representative traces showing changes in membrane-associated $[Ca^{2+}]$ of individual cells (F: fluorescent value at any time point; F_0: fluorescent value at $t = 0$) to KCl alone (a), KCl plus 10 μM nifedipine (b), 100 μM La^{3+} (c) and 10 μM SKF-96365 (d).

the activation of NOS associated with the surface membrane of human skeletal muscle cells.

RNS generation

The detection of NOS/RNS on the plasma membrane of human myotubes was carried out by immunohistochemistry in the TIRF mode. As can be seen in Figure 4A, NOS is distributed in distinct fluorescent dots or puncta, which are presumably localized on the surface membrane of the human myotube. The cells were also stained with anti-RyR1 Abs and monitored by epifluorescence (Fig. 4A). We next investigated whether ECCE activates the generation of RNS, by following the changes in the fluorescence of diacetate (4-amino-5-methylamino-2,7-difluorofluorescein) (DAF-FM) by TIRF microscopy. Previous studies have indicated high background fluorescence and relatively low signal-to-noise ratio when using conventional epifluorescence microscopy in

combination with DAF-FM (34). Using the same protocol utilized to stimulate ECCE, we show that RNS generation occurs in myotubes stimulated with KCl and that TIRF microscopy is suited to measure such localized events. Figure 4B shows time-lapse changes of DAF-FM fluorescence before the application of 100 mM KCl ($t = 0$) and 2, 5, 10 and 15 s after its application. The increase of DAF-FM fluorescence occurs on discrete areas of the surface membrane and since the localization and intensity of the DAF-FM signal exhibit remarkable variation within each cell, we measured the increase of the fluorescent signal over the entire footprint of cell (see Supplementary Material, Fig. S2, for a higher resolution image of the increase in DAF-FM fluorescence at 5 s after stimulation). As shown in Figure 4C, DAF-FM fluorescence shows a peak at 5 s after the addition of KCl and then decays rapidly to pre-stimulation levels. This increase in fluorescence could be prevented by pre-incubating myotubes with 50 μM of the NOS inhibitor L-NNA (35) during the loading
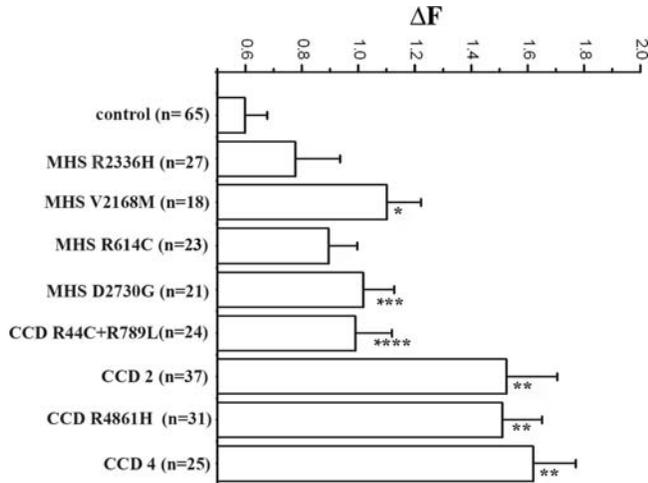
Figure 3. ECCE in human myotubes from control, MH and CCD patients. Experiments were performed in TIRF mode as outlined in Figure 2. Bar histograms show mean ($\pm$ SEM) peak Ca^{2+} increase induced by 100 mM KCl. Data from control myotubes are the mean ($\pm$ SEM) change in fluorescence measured in myotubes obtained from three control individuals. Statistical analysis was performed using the ANOVA test followed by Dunnett's *post hoc* test. *$P < 0.002$, **$P < 0.0001$, ***$P < 0.007$ and ****$P < 0.05$ compared with cells from control individuals.

procedure and throughout the experiment. Furthermore, omission of Ca^{2+} from the KCl solution also resulted in negligible RNS generation (Fig. 4D), indicating that this event depends on the influx of Ca^{2+} from the extracellular environment.

We next measured ECCE-dependent RNS formation in myotubes from three control individuals and in cells from MHS and CCD patients. Figure 5 summarizes the peak changes in DAF-FM fluorescence ($\triangle F$) in cells stimulated with 100 mM KCl. As shown, control cells produce negligible amounts of RNS, and the increases in fluorescence in the presence or absence of 50 μM L-NNA were not significantly different. On the other hand, myotubes from all MH and CCD patients (except for CCD myotubes bearing the R4861H mutation, where the variability was greater and did not reach statistical significance) produced significantly larger amounts of RNS during ECCE, compared with controls. Figure 5 also shows that the increase in DAF-FM fluorescence was largely prevented by L-NNA, indicating that it is due to the activation of NOS. Altogether, these results indicate a link between ECCE and RNS and show that myotubes from patients carrying *RYR1* mutations produce more NO radicals than cells from control individuals. The activation of NOS has been linked to the activation of gene transcription via nuclear translocation of calcium-dependent transcriptional factor(s) (36). In the next set of experiments, we examined the influence of ECCE on nuclear translocation of NFAT.

ECCE affects NFTAc1 nuclear translocation in muscle cells from CCD patients

NFTAc1 nuclear translocation is known to be an important step of the slow fibre-type differentiation programme (23,24). We focused on this isoform of NFAT since it was
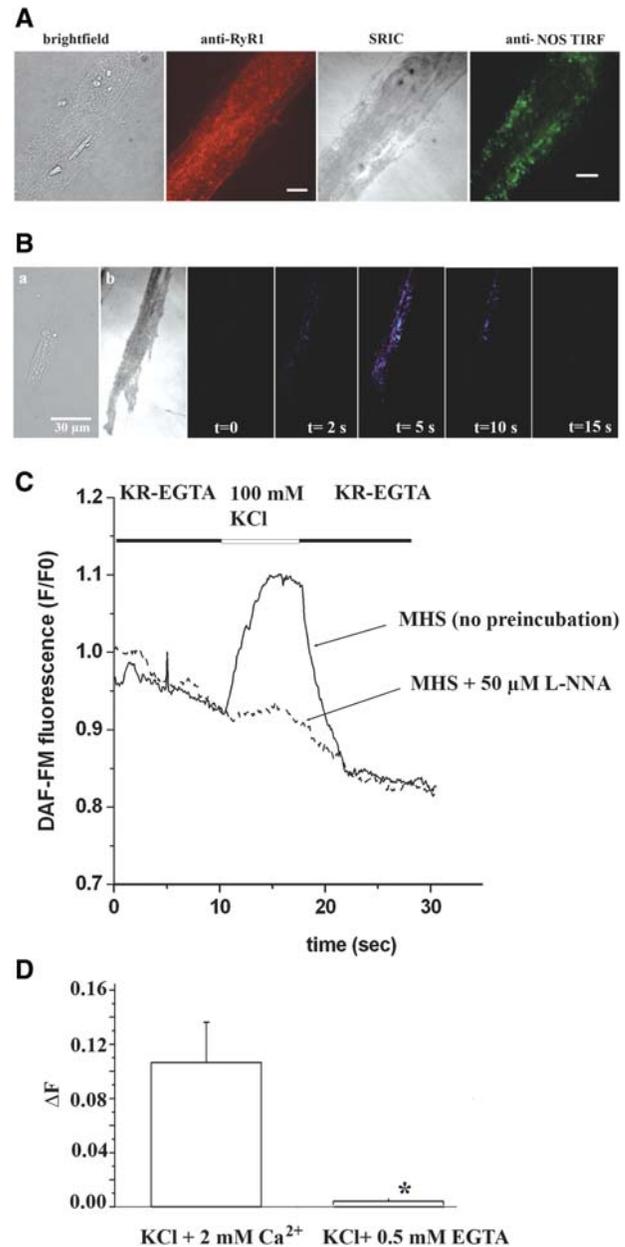
Figure 4. Depolarization-induced Ca^{2+} influx activates NOS. (**A**) Photomicropgraphs showing a human myotube stained for RyR and NOS. Left panel, brightfield; central left, epifluorescence showing anti-RyR1 staining; central right, SRIC filter; right, TIRF image of the same myotube showing discreet punctuated fluorescence on plasma membrane with anti-NOS. Images were acquired through a $100\times$ TIRF objective (1.45 NA). Bar indicates 20 μm. (**B**) Myotubes were loaded with the RNS-sensitive dye DAF-FM and visualized by brightfield (a), with an SRIC filter (b) and at the indicated time points after the addition of KCl. Images were acquired through a $60\times$ TIRF objective (1.49 NA). Panels show pseudo-coloured (Metamorph) micrographs of ratiometric changes (F/F_0) of DAF-FM fluorescence. Bar indicates 30 μm. (**C**) Representative traces showing changes in membrane-associated DAF-FM fluorescence in a cell from an MHS individual (F: fluorescent value at any time point; F_0: fluorescent value at $t = 0$) after the addition of 100 mM KCl in an untreated cell (continuous trace) and in a cell pre-treated with 50 μM of the NOS inhibitor L-NNA. (**D**) Mean ($\pm$ SEM) peak increase in DAF-FM fluorescence induced by 100 mM KCl in the presence ($n = 23$ cells analysed) or absence ($n = 15$ cells analysed) of extracellular Ca^{2+}. Statistical analysis was performed using Student's t-test; *$P < 0.001$.
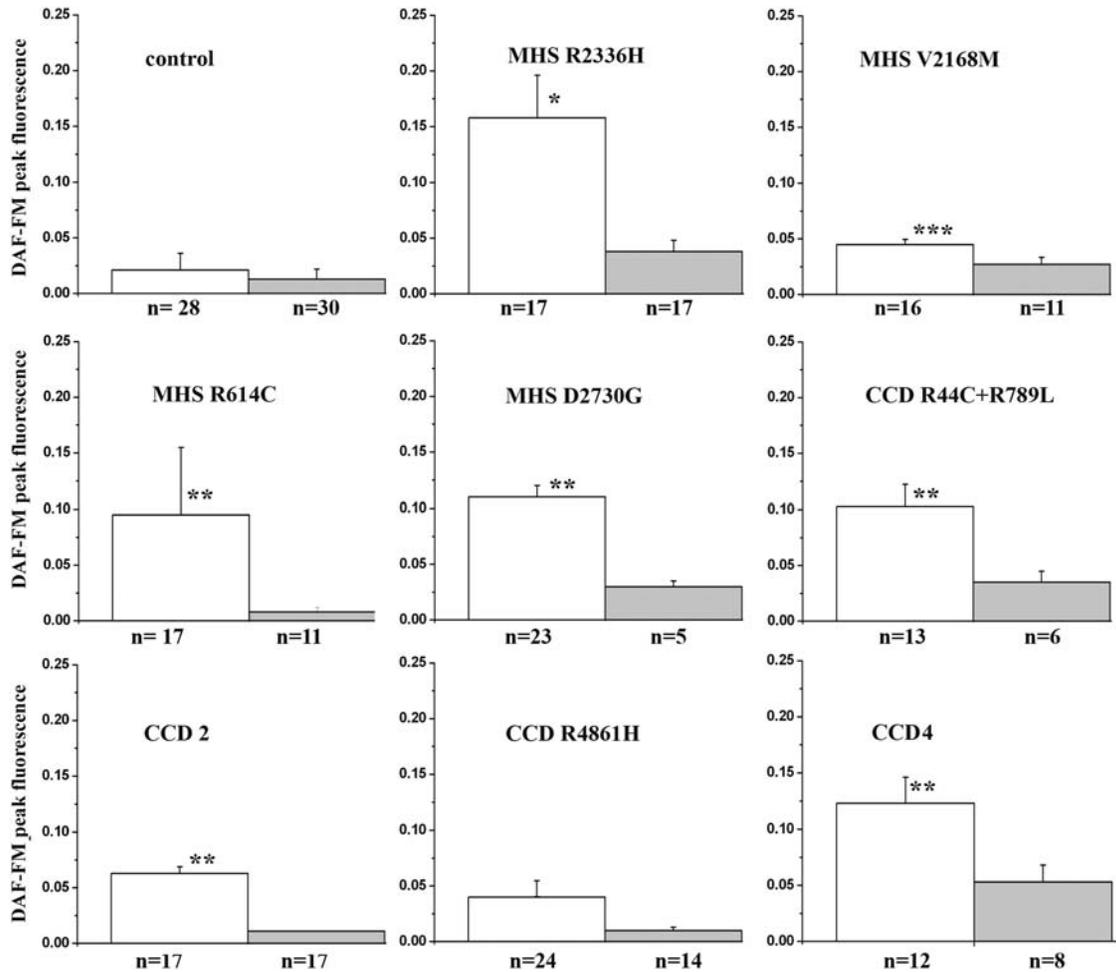
Figure 5. ECCE-induced RNS generation is increased in myotubes from MHS and CCD patients. Experiments were performed in TIRF mode as outlined in Figure 4. Bar histograms show mean ($\pm$ SEM) peak DAF-FM fluorescent increase induced by 100 mM KCl in untreated cells (white bars) and in cells pre-incubated for 30 min with 50 μM NOS inhibitor L-NNA. Statistical analysis was performed using the ANOVA test followed by Dunnett's *post hoc* test. $^*P < 0.015$, $^{**}P < 0.0001$, $^{***}P < 0.0003$ with respect to untreated cells from controls.

recently demonstrated that NFATc1 can be induced to translocate from the cytoplasm to the nucleus by treating myotubes with KCl and that sustained nuclear retention was promoted by external Ca^{2+} (37,38).

Figure 6A shows the subcellular distribution of NFATc1 in myotubes from control and CCD patients after treatment with 60 mM KCl. KCl-induced depolarization of ryanodine-treated cells is deemed to increase Ca^{2+} influx into myotubes (as shown in Figs 2 and 3), an event which affects the subcellular distribution of NFATc1. As expected, stimulation of Ca^{2+} influx is accompanied by an increase of the nuclear distribution of NFATc1. The nuclear/cytoplasm fluorescence ratio of NFATc1 was significantly higher and remained elevated after 5 and 30 min of KCl stimulation, in myotubes from the CCD patients (Fig. 6B, left panel), a result consistent with the larger extent of ECCE in these myotubes compared with that of cells from controls. It should also be pointed out that the NFAT nuclear-to-cytoplasmic ratio was already slightly but significantly elevated in unstimulated myotubes from CCD patients. When KCl plus 100 μM La^{3+} was added to cells from CCD patients, the nucleus/cytoplasmic fluorescent

ratio was significantly reduced; similarly, pre-treatment of myotubes from CCD patients with L-NNA significantly reduced the nuclear translocation of NFATc1 (Fig. 6B, right panel). Finally, addition of 600 μM 4-chloro-*m*-cresol, a direct pharmacological RyR1 activator, had a negligible effect on NFAT translocation in CCD myotubes (Fig. 6B, right panel), indicating that depolarization of CCD myotubes causes NFAT translocation mainly by activating influx of Ca^{2+}.

These results suggest that some genes under the control of the transcriptional factor NFATc1 might be up-regulated in muscles from CCD individuals. Among many such genes, we focused on that encoding IL-6 since previous reports have demonstrated a link between Ca^{2+}, *RYR1* mutations and IL-6 release (8). We next studied the effect of KCl-induced depolarization on IL-6 release from myotubes from controls and CCD patients. In the presence of 2 mM Ca^{2+}, treatment of myotubes from control individuals with 60 mM KCl resulted in a significant release of IL-6, which was blocked when the experiment was performed in the presence of 100 μM La^{3+} (Fig. 6C), supporting the hypothesis that
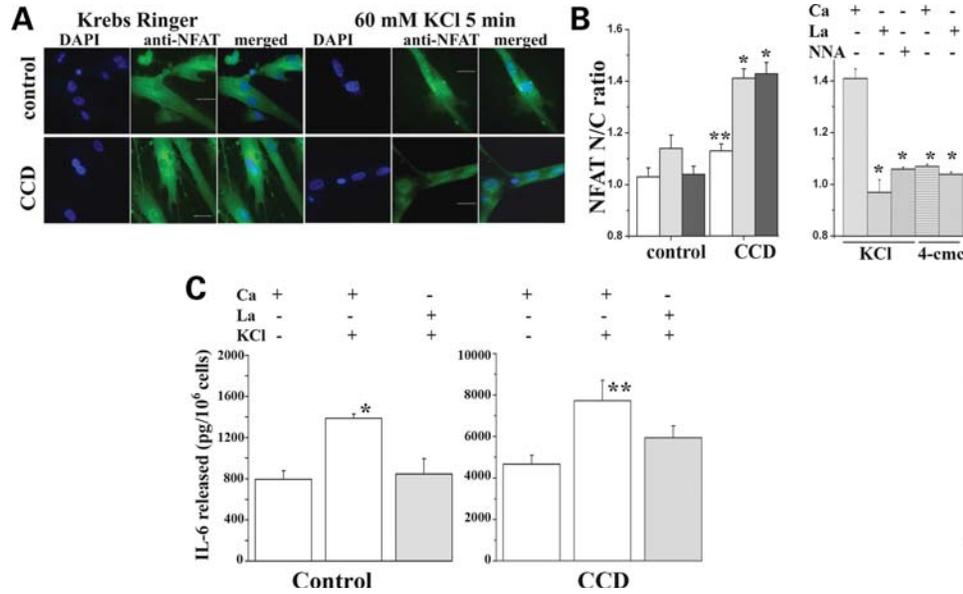
Figure 6. ECCE induces NFAT nuclear translocation and enhances IL-6 release by myotubes from CCD patients. (**A**) Myotubes from a control and CCD individuals were pre-treated with 500 μM ryanodine and incubated in Krebs–Ringer solution or with 60 mM KCl for 5 min at 37°C. Cells were immediately fixed with ice-cold methanol:acetone (1:1) and processed for immunofluorescence as described in Materials and Methods. Images (60× TIRF objective) show epifluorescence using anti-NFATc1 Ab (green) and DAPI (blue) for nuclear staining. Bar: 30 μm. (**B**) Left panel: bar histograms showing the nuclear-to-cytoplasm NFAT fluorescence intensity in cells from three different control individuals (*n* ranged between 25 and 35 individual cells) and two different CCD individuals (*n* ranged between 35 and 38 individual cells) in untreated cells (white bars) and cells treated for 5 min (light grey) and 30 min (dark grey) with 60 mM KCl plus 2 mM Ca^{2+}. Right panel: bar histograms showing the nuclear-to-cytoplasm NFAT fluorescence intensity in cells from two different CCD individuals in (i) cells pre-treated with ryanodine, and stimulated 5 min with KCl in the presence of 2 mM Ca^{2+}, 100 μM La^{3+}, or pre-treated with 50 μM L-NNA + 2 mM Ca^{2+}, or (ii) in non-ryanodine pre-treated cells, stimulated for 5 min with 600 μM 4-chloro-*m*-cresol in the presence of 2 mM Ca^{2+} or 100 μM La^{3+} (*n* ranged between 19 and 70 individual cells). The area over the nucleus was selected by using the DAPI image and transferred to the NFAT fluorescence image using the 'transfer region option' of the Metamorph software package. Average fluorescent intensity in nuclei and region excluding nuclei was calculated with Metamorph. Only myotubes containing more than two nuclei were included and the average fluorescent intensity of all the nuclei of one cell was averaged per cell. **$P < 0.03$, *$P < 0.0001$ compared with controls. (**C**) IL-6 release induced by 60 mM KCl from myotubes from two control individuals (scale bar from 0 to 2000 pg/10⁶ cells) and in myotubes from two CCD patients (scale bar from 0 to 10 000 pg/10⁶ cells). After 30 min of incubation with 60 mM KCl, the medium was replaced by differentiation medium and cells were incubated at 37°C for four additional hours. The amount of IL-6 released was quantified as described in Materials and Methods. Bar histograms show the mean (± SEM) of 7–15 measurements. Statistical analysis was performed using the ANOVA followed by Dunnett's *post hoc* test. **$P < 0.02$ and *$P < 0.0007$.

Ca^{2+} influx plays a role in KCl-induced IL-6 release from myotubes. Myotubes obtained from CCD patients released IL-6 to a much higher extent compared with control cells (note that the IL-6 scale bars are different between controls and CCD patients) (Fig. 6C, right panel). IL-6 is released from CCD myotubes in the absence of KCl, and the addition of 60 mM KCl + 2 mM Ca^{2+} results in a further release of IL-6. The latter event was partially reversed when the experiment was performed in the absence of added Ca^{2+} and in the presence of 100 μM La^{3+}. These results suggest that depolarization-induced IL-6 release from human myotubes is mediated, at least in part, by the influx of extracellular Ca^{2+}.

DISCUSSION

In the present study, we show that cultured myotubes from patients with MH and CCD have an altered ECCE. In particular, ECCE is enhanced to a much greater extent in cells from patients with CCD compared with those with MH and control individuals. We also show that the Ca^{2+} influx via ECCE has at least two physiological effects: it induces (i) generation of RNS via the activation of NOS expressed in myotubes, and (ii) nuclear translocation of the Ca^{2+}-sensitive transcription

factor NFAT. The dysregulation of Ca^{2+} homeostasis seen in myotubes from CCD patients (increase of the resting $[Ca^{2+}]$ and increased Ca^{2+}-influx) leads to downstream effects such as to the nuclear translocation of the transcription factor NFAT and to higher levels of IL-6 release.

Analysis of calcium influx of human myotubes from MH and CCD patients by TIRF microscopy

A great deal of data (8,13,21,32,39) have shown that a number *RYR1* mutations cause the expression of leaky channels in myotubes from MH and CCD patients and this is associated with an elevation of the resting $[Ca^{2+}]$. This increased Ca^{2+} leak via mutant *RYR1*s might also be associated with defect(s) in the regulation of the plasma membrane Ca^{2+} influx pathways, whereby the long-term Ca^{2+} store-refilling process is affected. In this study, we monitored for the first time calcium influx in myotubes expressing naturally occurring *RYR1* mutants from CCD and MH patients, by exploiting TIRF microscopy, the state-of-the-art technology to monitor fluorescent signals with a high signal-to-noise ratio from a 100 nm thick optical section localized on or very close to the plasma membrane. Cherednichenko *et al.* (18) suggested

that muscle cell depolarization not only triggers Ca^{2+} release, but also calcium entry via ECCE and that the latter event requires the interaction of the DHPR with the RyR. These results imply that the molecular physiology of ECCE might be affected by mutations in the DHPR and/or RyR1. The results reported here support and extend this idea. We found that the expression of *RYR1* mutations linked to both MH and CCD induced an increase of ECCE which is most likely not due to changes in the expression level of the $Ca_v1.1$ transcript. In particular, we found that the enhancement of ECCE appears to be correlated with the effect of the RyR mutant on the resting calcium concentration. The myotubes expressing leaky RyR mutants which are associated with a significantly higher resting $[Ca^{2+}]$ also had a significantly larger ECCE (compare Figs 1A and 3). These results are consistent with the idea that variations of the resting $[Ca^{2+}]$ cannot be ascribed to a change in calcium fluxes across SR(ER) membranes only, unless they also cause changes of calcium fluxes at the level of the plasma membrane (17). Myotubes from MHS/CCD patients may adapt to the presence of mutations in the *RYR1* by increasing Ca^{2+} influx across the sarcolemma. The increased ECCE may be a compensatory mechanism particularly relevant in CCD patients to cope with the low levels of Ca^{2+} released from the SR during T-tubule depolarization.

NOS activation by ECCE

The enhancement of ECCE, which is particularly relevant in CCD patients, may affect the activity of membrane-bound enzymes allosterically regulated by calcium. In this context, it is worth mentioning that eNOS and nNOS, the two nitric oxide synthase isoforms, are constitutively expressed in skeletal muscles (25), are Ca^{2+}-sensitive and are activated by skeletal muscle contraction. Depletion of intracellular Ca^{2+} stores has been shown to activate NOS in a number of cell types (40,41). We hypothesized that one of the functions of ECCE may be to activate the Ca^{2+}-sensitive NOS in myotubes, leading to the generation of the second messenger and free radical NO. Indeed, Durham *et al.* (33) recently suggested that in the MHS *RYR1* knock in Y522S mouse model, generation of RNS is linked to Ca^{2+} leak from the SR, and this leads to heat stroke and sudden death. By exploiting the RNS indicator DAF-FM and the same protocol used to measure ECCE, we demonstrate that ECCE leads to the generation of RNS. We are confident that the DAF-FM signal is due to Ca^{2+}-dependent NOS activation since it was inhibited by the NOS inhibitor L-NNA (35) and by preventing calcium entry with extracellular Ca^{2+} chelators. Although measurements of RNS production by DAF-FM dye in epifluorescence mode have shown an irreversible increase of the fluorescent signal, in our experimental setting we found that the DAF-FM fluorescent signal is reversible. A number of reasons may account for the decay of the DAF-FM signal. As reported previously by Sheng *et al.* (42), when measuring NO synthesis in vascular endothelial cells, the dye may bleach during excitation, especially with the powerful Sapphire laser we used in the present experiments. The second possibility is also linked to our experimental set up. We think that the decay of DAF-FM signal is indicative of the diffusion of the dye away from the TIRF focal plane. Contrary to our expectations

however, the overall peak DAF-FM fluorescent increase was larger in cells from MHS individuals compared with that observed in cells from CCD patients, even though the latter showed significantly higher ECCE. An investigation on the Ca^{2+} dependence of NOS activation (43) showed that at a pH of 7.1, formation of NO by NOS has a bell-shaped curve, with maximal activity between 1 and 100 μM and thereafter the activity is drastically reduced. Furthermore, the activity of NOS increases greatly with variations in $[Ca^{2+}]$ over the physiological range, i.e. between 100 and 200 nM (43). Additionally, Schmidt *et al.* (44) showed that long-lasting increases in Ca^{2+} down-regulate NO formation. Thus, the enhanced Ca^{2+} influx triggered in myotubes derived from CCD patients may affect the enzymatic activity of NOS, leading to lower amounts of NO formation as observed in cells from CCD patients compared with those from MHS individuals.

NFAT gene expression and ECCE

As to the subcellular distribution of the Ca^{2+}-sensitive transcription factor NFAT, our results are in agreement with previous reports showing that in cultured myotubes the c1 isoform of NFAT translocates to the nuclei in a Ca^{2+}-dependent manner and that K^+-induced depolarization and electrical stimulation induce nuclear translocation of NFATc1 and that extracelluar Ca^{2+} contributes to the activation of NFAT (37,38,45). In fact, we found that ECCE-induced nuclear translocation of NFAT was more pronounced in myotubes from the CCD patients compared with myotubes from controls. Interestingly, nuclear distribution of NFATc1 in adult skeletal muscle fibres appears to be an important step of the slow fibre-type differentiation programme (24,46) and this is consistent with the fibre type-1 predominance observed in CCD patients. The present report indicates that stimulation of NOS is involved in the NFAT-dependent transcription activity in human myotubes, a conclusion in agreement with data provided by Drenning *et al.* (36), who showed that NO enhances Ca^{2+}-dependent nuclear accumulation and transcriptional activity of NFAT in mouse muscle cells. We have previously demonstrated that the release of IL-6 from cultured human myotubes is Ca^{2+} dependent and is inhibited by cyclosporine, a blocker of the NFAT pathway (8). The involvement of NFAT in the activation of IL-6 is consistent with (i) the presence of NFAT-responsive elements in the promoter of the human IL-6 gene (47), and with (ii) the inhibition of IL-6 production in vascular human smooth muscle cells by a specific NFAT blocker (48). In the present report, we confirm and extend these observations and show that IL-6 release from human myotubes *in vitro* is mediated by two components: one is dependent on the elevated resting $[Ca^{2+}]$ and the other is dependent on the influx of extracellular calcium induced by prolonged membrane depolarization.

In conclusion, we believe RyR mutations causing alterations of Ca^{2+} homeostasis via leaky RyR channels and/or enhanced ECCE also lead to an up-regulation of 'NFAT-dependent pathways' resulting in an increased release of the pro-inflammatory cytokine IL-6. Future studies aimed at understanding the roles of IL-6 in muscle cell physiology and the implications of its enhanced release from cells from

patients with CCD and other neuromuscular disorders may help shed light into some of the pathological alterations seen in patients with ryanodinopathies such as muscle cramping and muscle protein breakdown (49,50).

MATERIALS AND METHODS

Materials

Dulbecco's modified Eagle's medium (DMEM) containing 4.5 mg/ml of glucose, penicillin G, streptomycin, Fluo-4/AM and DAF-FM, AlexaFluor 488-conjugated chicken anti-rabbit IgG, AlexaFluor 568-conjugated donkey anti-mouse IgG and 4′,6-diamidino-2-phenylindole, dihydrochloride (DAPI) were from Life Technologies, Ltd. Insulin was purchased from Eli Lilly and Company, Indianapolis, IN, USA. Cell culture plastic ware was from Becton Dickinson. Glutamine, HEPES, BSA, EGF, SKF-96365 creatine anti-α-actinin Abs were from Sigma Chemical. Fura-2/AM, nifedipine and ryanodine were from Calbiochem. Rabbit anti-NFATc1 (sc-13033), goat anti-NOS (sc-49058) and FITC-conjugated donkey anti-goat IgG were from Santa Cruz Biotechnology. Mouse anti-RyR Abs were from Affinity Bioreagents. IL-6 was determined by ELISA using the PeliPair reagent kit Sanquin reagents (The Netherlands). Qualitative determination of CRP was performed using the Humatex kit (HUMAN Gesellschaft für Biochemica und Diagnostica mbH, Wiesbaden, Germany). All other chemicals were reagents of highest available grade.

Human muscle cells

Primary muscle cell cultures were established from fragments of muscles obtained from biopsies of patients undergoing diagnostic testing for MH (4 MHS), from patients diagnosed as CCD from Genethon (Institut de Myologie, Paris, France) and CHUV (Lausanne, Switzerland), as described previously (8). Mutation screening confirmed the presence of the following *RYR1* mutations which have been associated with the MHS phenotype: c.7007G > A (p.R2336H) (51), c.6502G > A (p.V2168M) (8,11), c.1840C > T (p.R614C) (11) and c.8189A > G (p.D2730G) (51). One CCD patient was heterozygous for the newly identified substitutions c.130C > T and c.2366G > T (p.R44C + p.R789L), whereas the other was heterozygous for the CCD-linked (10,11,16) c.14582G > A mutation (p.R4861H). Molecular genetic analysis performed by sequencing genomic DNA from the other two CCD patients failed to identify any *RYR1* substitution though, based on their neurological and histological examinations, they were clinically classified as CCD patients. Cells were cultured on 0.17 mm thick glass coverslips in growth medium and induced to differentiate into myotubes by culturing them in differentiation medium (DMEM plus 4.5 mg/ml glucose, 0.5% BSA, 10 ng/ml EGF, 0.15 mg/ml creatine, 5 ng/ml insulin, 200 mM glutamine, 600 ng/ml penicillin G and streptomycin, and 7 mM HEPES, pH 7.4) for 7–10 days.

Calcium measurements

Myotubes were loaded with fura-2 or fluo-4 (final concentration 5 μM) in differentiation medium for 30 min at 37°C, after which the coverslips were mounted onto a 37°C thermostatically controlled chamber which was continuously perfused with Krebs–Ringer medium; individual cells were stimulated by means of a 12- or 8-way 100 mm diameter quartz micromanifold computer-controlled microperfuser (ALA Scientific Instruments, Westbury, NY, USA), as described previously (8). (i) For global changes in the intracellular Ca^{2+} concentration, the fluorescent ratiometric Ca^{2+} indicator fura-2 was used. Online measurements were recorded using a fluorescent Axiovert S100 TV inverted microscope (Carl Zeiss GmbH, Jena, Germany) equipped with a $20\times$ water-immersion FLUAR objective (0.17 NA) and filters (BP 340/380, FT 425, BP 500/530) and attached to a Hamamatsu multiformat CCD camera. Changes in fluorescence were analysed using an Openlab imaging system and the average pixel value for each cell was measured at excitation wavelengths of 340 and 380 nm as described previously (8). (ii) The dynamics of $[Ca^{2+}]$ influx were investigated by TIRF microscopy using the fast Ca^{2+} indicator Fluo-4 as described previously (52). Glass coverslip grown and differentiated human myotubes were mounted on a thermostated perfusion chamber, bathed continuously in Krebs–Ringer. ECCE was measured after the application of 100 mM KCl to myotubes pre-treated with 500 μM ryanodine to block RyR1-mediated Ca^{2+} release. Online fluorescence images were acquired using an inverted Nikon TE2000 TIRF microscope equipped with an oil immersion CFI Plan Apochromat $60\times$ TIRF objective (1.49 NA) and an electron multiplier Hamamatsu CCD camera C9100–13 which allows fast data acquisition. Our TIRF microscope is equipped with an SRIC cube in order to maintain the focal plane at the coverglass/cell membrane contact prior to and during TIRF acquisition. The focus was maintained at the coverglass/cell membrane contact by using the PFS that exploits an infrared laser beam and a quadrant diode for the online control of the microscope's focusing motor. Fluo-4 loaded cells were excited with a solid-state laser beam at 488 nm and the emitted fluorescence was collected through a 520 narrow-band filter. Data were analysed using Metamorph imaging software (Molecular Devices).

Real-time PCR

At the end of the Ca^{2+} measurement experiments, myotubes from controls, MH and CCD patients were scraped off the glass coverslips, pelleted and stored in liquid nitrogen. Total RNA was extracted (Qiagen, Basel, Switzerland) and treated with deoxyribonuclease I (Invitrogen, Carlsbad, CA, USA). After reverse transcription using 500 ng of RNA (high-capacity cDNA reverse transcription kit, Applied Biosystems, Forster City, CA, USA), cDNA was amplified by quantitative real-time PCR using SYBR Green technology (Fast SYBR Green Master Mix, Applied Biosystem) as described previously (52) and the following primers: β-actin (forward 5′-CATGTACGTTGCTATCCAGGC-3′ and reverse 5′-CTCCTTAATGTCACGCACGAT-3′), desmin (forward 5′-AACCAGGAGTTTCTGACCACG-3′ and reverse 5′-TTG AGCCGGTTCACTTCGG-3′), Ca$_v$1.1 (forward 5′-ATGAC GACCTACGGAGCCTT-3′ and reverse 5′-ACGAACATGC ACCTAGCCAC-3′). Gene expression was verified using

β-actin as a housekeeping gene and normalized for the early myotube differentiation marker desmin as reference for myotubes content. $Ca_v1.1$ gene expression in MH and CCD myotubes was calculated as a fold increase compared with that observed in myotubes from control individuals.

Reactive nitrogen species

The generation of RNS was followed by monitoring the increase in fluorescence of the dye DAF-FM at $37^{\circ}C$ (34,40). Briefly, coverslip grown and differentiated myotubes were loaded with 10 μM DAF-FM for 30 min at $37^{\circ}C$ in differentiation medium in the presence of 500 μM ryanodine. Coverslips were transferred onto the stage of a Nikon Eclipse TE2000-E fluorescent microscope; the cells were excited at 488 nm and the emission was followed at 510 nm as described above for fluo-4 measurements.

Immunofluorescence

Indirect immunofluorescence was performed on methanol:acetone (1:1)-fixed myotubes using rabbit anti-NFATc1 (final concentration 10 μg/ml), goat anti-NOS, mouse anti-RyR, followed by the appropriate fluorescently labelled secondary antibodies. Nuclei were visualized by counterstaining with DAPI (100 μM) prior to mounting the coverslips. For experiments monitoring NFAT localization, cells were either unstimulated, incubated with 500 μM ryanodine and stimulated with 60 mM KCl as indicated or stimulated with 600 μM 4-chloro-*m*-cresol without ryanodine pre-treatment. Cells were then fixed as described above and NFAT localization was monitored by epifluorescence through an oil immersion CFI Plan Apochromat $60\times$ TIRF objective (1.49 NA) using appropriate filters for FITC and DAPI detection and processed as described below using the Metamorph (Molecular Devices) 5.7.4 software package. First, the area around the nucleus was selected as a 'region of interest' using the DAPI image and transferred to the NFAT fluorescence image using the 'transfer region' option. The average fluorescent intensity in nuclei and region excluding nuclei was averaged and the ratio of the intensity in the nucleus to cytoplasm was calculated. Only myotubes containing more than two nuclei were included. For NOS, surface fluorescence was monitored by means of an oil immersion CFI Plan Apochromat $100\times$ TIRF objective; the focal plane at the coverglass/cell membrane contact was first visualized with the SRIC cube and this focal plane was maintained with the PFS.

IL-6 release from myotubes

IL-6 release from human myotubes (two control individuals and two CCD patients) was performed as described previously (8) except that cells were stimulated with 60 mM KCl in the presence of 2 mM Ca^{2+} or in the presence of 100 μM La^{3+} or incubated with Krebs–Ringer ($+2$ mM Ca^{2+}) at $37^{\circ}C$. After 30 min, the medium containing 60 mM KCl was replaced by differentiation medium and the cells were incubated at $37^{\circ}C$ for an additional 4 h. The culture medium was then harvested, centrifuged to remove any cell debris or cells which may have detached during the incubation, and the supernatant

(200 μl) was assayed for IL-6 by ELISA using the PeliPair reagent kit following the manufacturer's recommendations.

Statistical analysis

Statistical analysis was performed using Student's *t*-test for two populations. When more than two samples were compared, analysis was performed by the ANOVA test followed by Dunnett's *post hoc* test, which is specifically designed for situations where all groups are to be compared against one 'reference' group. The PROC MIXED statistical analysis program (SAS 9.2) was used for statistical analysis. Values were considered significant when $P < 0.05$.

SUPPLEMENTARY MATERIAL

Supplementary Material is available at *HMG* online.

REFERENCES

1. Fleischer, S. and Inui, M. (1989) Biochemistry and biophysics of excitation–contraction coupling. *Annu. Rev. Biophys. Biophys. Chem.*, **18**, 333–364.
2. Rios, E. and Pizarro, G. (1991) Voltage sensor of excitation–contraction coupling in skeletal muscle. *Physiol. Rev.*, **71**, 849–908.
3. Franzini-Armstrong, C. and Jorgensen, A.O. (1994) Structure and development of E–C coupling units in skeletal muscle. *Annu. Rev. Physiol.*, **56**, 509–534.
4. Sutko, J.L. and Airey, J.A. (1996) Ryanodine receptor Ca^{2+} release channels: does diversity in form equal diversity in function? *Physiol. Rev.*, **76**, 1027–1071.
5. Nakai, J., Dirksen, R.T., Nguyen, H.T., Pessah, I.N., Beam, K.G. and Allen, P.D. (1996) Enhanced dihydropyridine receptor channel activity in the presence of ryanodine receptor. *Nature*, **380**, 72–75.
6. Wilmshurst, J.M., Lillis, S., Zhou, H., Pillay, K., Henderson, H., Kress, W., Müller, C.R., Ndondo, A., Cloke, V., Cullup, T. *et al.* (2010) RYR1 mutations are a common cause of congenital myopathies with central nuclei. *Ann. Neurol.*, **68**, 717–726.
7. Clarke, N.F., Waddell, L.B., Cooper, S.T., Perry, M., Smith, R.L., Kornberg, A.J., Muntoni, F., Lillis, S., Straub, V., Bushby, K. *et al.* (2010) Recessive mutations in RYR1 are a common cause of congenital fiber type disproportion. *Hum. Mutat.*, **31**, E1544–E1550.

8. Ducreux, S., Zorzato, F., Müller, C., Sewry, C., Muntoni, F., Quinlivan, R., Restagno, G., Girard, T. and Treves, S. (2004) Effect of ryanodine receptor mutations on IL-6 release and intracellular calcium homeostasis in human myotubes from malignant hyperthermia susceptible individuals and patients affected by central core disease. *J. Biol. Chem.*, **279**, 43838–43846.

9. Lynch, P.J., Tong, J., Lehane, M., Mallet, A., Giblin, L., Heffron, J.J., Vaughan, P., Zafra, G., MacLennan, D.H. and McCarthy, T.V. (1999) A mutation in the transmembrane/luminal domain of the ryanodine receptor is associated with abnormal Ca^{2+} release channel function and severe central core disease. *Proc. Natl Acad. Sci. USA*, **96**, 4164–4169.

10. Tilgen, N., Zorzato, F., Halliger-Keller, B., Muntoni, F., Sewry, C., Palmucci, L.M., Schneider, C., Hauser, E., Lehmann-Horn, F., Müller, C.R. and Treves, S. (2001) Identification of four novel mutations in the C-terminal membrane spanning domain of the ryanodine receptor 1: association with central core disease and alteration of calcium homeostasis. *Hum. Mol. Genet.*, **10**, 2879–2887.

11. Treves, S., Anderson, A.A., Ducreux, S., Divet, A., Bleunven, C., Grasso, C., Paesante, S. and Zorzato, F. (2005) Ryanodine receptor 1 mutations, dysregulation of calcium homeostasis and neuromuscular disorders. *Neuromuscul. Disord.*, **15**, 577–587.

12. Avila, G., O'Brien, J.J. and Dirksen, R.T. (2001) Excitation–contraction uncoupling by a human central core disease mutation in the ryanodine receptor. *Proc. Natl Acad. Sci. USA*, **98**, 4215–4220.

13. Avila, G. and Dirksen, R.T. (2001) Functional effects of central core disease mutations in the cytoplasmic region of the skeletal muscle ryanodine receptor. *J. Gen. Physiol.*, **118**, 277–290.

14. Avila, G., O'Connell, K. and Dirksen, R.T. (2003) The pore region of the skeletal muscle ryanodine receptor is a primary locus for excitation–contraction uncoupling in central core disease. *J. Gen. Physiol.*, **121**, 277–286.

15. Dirksen, R.T. and Avila, G. (2004) Distinct effects on Ca^{2+} handling caused by malignant hyperthermia and central core disease mutations in RyR1. *Biophys. J.*, **87**, 3193–3204.

16. Treves, S., Jungbluth, H., Muntoni, F. and Zorzato, F. (2008) Congenital muscle disorders with cores: the ryanodine receptor calcium channel paradigm. *Curr. Opin. Pharmacol.*, **8**, 319–326.

17. Rios, E. (2010) The cell boundary theorem: a simple law of the control of cytosolic calcium concentration. *J. Physiol. Sci.*, **60**, 81–84.

18. Cherednichenko, G., Hurne, A.M., Fessenden, J.D., Lee, E.H., Allen, P.D., Beam, K.G. and Pessah, I.N. (2004) Conformational activation of calcium entry by depolarisation of skeletal muscle myotubes. *Proc. Natl Acad. Sci. USA*, **101**, 15793–15798.

19. Bannister, R.A., Pessah, I.N. and Beam, K.G. (2008) The skeletal L-type Ca^{2+} current is a major contributor to excitation-coupled Ca^{2+} entry. *J. Gen. Physiol.*, **133**, 79–91.

20. Cherednichenko, G., Ward, C.W., Feng, W., Cabrales, E., Michaelson, L., Samso, M., López, J.R., Allen, P.D. and Pessah, I.N. (2008) Enhanced excitation-coupled calcium entry (ECCE) in myotubes expressing malignant hyperthermia mutation R163C is attenuated by dantrolene. *Mol. Pharmacol.*, **73**, 1203–1212.

21. Yang, T., Allen, P.D., Pessah, I.N. and Lopez, J.R. (2007) Enhanced excitation-coupled calcium entry in myotubes is associated with expression of RyR1 malignant hyperthermia mutations. *J. Biol. Chem.*, **282**, 37471–37478.

22. Dirksen, R.T. (2009) Checking your SOCCs and feet: the molecular mechanisms of Ca^{2+} entry in skeletal muscle. *J. Physiol.*, **587**, 3139–3147.

23. Olson, E.N. and Williams, R.S. (2000) Remodeling muscles with calcineurin. *Bioessays*, **22**, 510–519.

24. Liu, Y., Randall, W.R. and Schneider, M.F. (2005) Activity-dependent and -independent nuclear fluxes of HDAC4 mediated by different kinases in adult skeletal muscle. *J. Cell. Biol.*, **168**, 887–897.

25. Stamler, J.S. and Meissner, G. (2001) Physiology of nitric oxide in skeletal muscle. *Physiol. Rev.*, **81**, 209–237.

26. Zhou, H., Yamaguchi, N., Xu, L., Wang, Y., Sewry, C., Jungbluth, H., Zorzato, F., Bertini, E., Muntoni, F., Meissner, G. and Treves, S. (2006) Characterization of recessive RYR1 mutations in core myopathies. *Hum. Mol. Genet.*, **15**, 2791–2803.

27. Yang, T., Esteve, E., Pessah, I.N., Molinski, T.F., Allen, P.D. and López, J.R. (2007) Elevated resting [Ca(2+)](i) in myotubes expressing malignant hyperthermia RyR1 cDNAs is partially restored by modulation

28. Reck-Peterson, S.L., Derr, N.D. and Stuurman, N. (2010) Imaging single molecules using total internal reflection fluorescence microscopy (TIRFM). *Cold. Spring. Harb. Protoc.*, [Epub a head of print].

29. Meissner, G. (1986) Ryanodine activation and inhibition of the Ca^{2+} release channel of sarcoplasmic reticulum. *J. Biol. Chem.*, **261**, 6300–6306.

30. Zimányi, I., Buck, E., Abramson, J.J., Mack, M.M. and Pessah, I.N. (1992) Ryanodine induces persistent inactivation of the Ca^{2+} release channel from skeletal muscle sarcoplasmic reticulum. *Mol. Pharmacol.*, **42**, 1049–1067.

31. Catterall, W.A., Perez-Reyes, E., Snutch, T.P. and Striessnig, J. (2005) International Union of Pharmacology. XLVIII. Nomenclature and structure–function relationships of voltage-gated calcium channels. *Pharmacol. Rev.*, **57**, 411–425.

32. Leung, Y.M. and Kwan, C.Y. (1999) Current perspectives in the pharmacological studies of store-operated Ca^{2+} entry blockers. *Jpn J. Pharmacol.*, **81**, 253–258.

33. Durham, W.J., Aracena-Parks, P., Long, C., Rossi, A.E., Goonasekera, S.A., Boncompagni, S., Galvan, D.L., Gilman, C.P., Baker, M.R., Shirokova, N. *et al.* (2008) RyR1 S-nitrosylation underlies environmental heat stroke and sudden death in Y522S RyR1 knockin mice. *Cell*, **133**, 53–65.

34. Leikert, J.F., Räthel, T.R., Müller, C., Vollmar, A.M. and Dirsch, V.M. (2001) Reliable *in vitro* measurement of nitric oxide released from endothelial cells using low concentrations of the fluorescent probe 4,5-diaminofluorescein. *FEBS Lett.*, **506**, 131–134.

35. Furfine, E.S., Harmon, M.F., Paith, J.E. and Garvey, E.P. (1993) Selective inhibition of constitutive nitric oxide synthase by L-NG-nitroarginine. *Biochemistry*, **32**, 8512–8517.

36. Drenning, J.A., Lira, V.A., Simmons, C.G., Soltow, Q.A., Sellman, J.E. and Criswell, D.S. (2008) Nitric oxide facilitates NFAT-dependent transcription in mouse myotubes. *Am. J. Physiol. Cell. Physiol.*, **294**, C1088–C1095.

37. Valdés, J.A., Gaggero, E., Hidalgo, J., Leal, N., Jaimovich, E. and Carrasco, M.A. (2008) NFAT activation by membrane potential follows a calcium pathway distinct from other activity-related transcription factors in skeletal muscle cells. *Am. J. Physiol. Cell. Physiol.*, **294**, C715–C725.

38. Rosenberg, P., Hawkins, A., Stiber, J., Shelton, J.M., Hutcheson, K., Basel-Duby, R., Shin, D.M., Yan, Z. and Williams, R.S. (2004) TRPC3 channels confer cellular memory of recent neuromuscular activity. *Proc. Natl Acad. Sci. USA*, **101**, 9387–9392.

39. López, J.R., Linares, N., Pessah, I.N. and Allen, P.D. (2005) Enhanced response to caffeine and 4-chloro-m-cresol in malignant hyperthermia-susceptible muscle is related in part to chronically elevated resting $[Ca^{2+}]_i$. *Am. J. Physiol. Cell. Physiol.*, **288**, C606–C612.

40. Parekh, A. and Penner, R. (1997) Store depletion and calcium influx. *Physiol. Rev.*, **77**, 901–926.

41. Xu, X., Star, R.A., Tortorici, G. and Muallem, S. (1994) Depletion of intracellular Ca^{2+} stores activates nitric oxide synthase to generate cGMP and regulate Ca^{2+} influx. *J. Biol. Chem.*, **269**, 12645–12653.

42. Sheng, J.Z., Wang, D. and Braun, A.P. (2005) DAF-FM (4-amino-5-methylamino-2′,7′-difluorofluorescein) diacetate detects impairment of agonist-stimulated nitric oxide synthesis by elevated glucose in human vascular endothelial cells: reversal by vitamin C and L-sepiapterin. *J. Pharmacol. Exp. Ther.*, **315**, 931–940.

43. Conte, A. (2003) Physiologic pH changes modulate calcium ion dependence of brain nitric oxide synthase in *Carassius auratus*. *Biochim. Biophys. Acta*, **1619**, 29–38.

44. Schmidt, H.H., Pollock, J.S., Nakane, M., Förstermann, U. and Murad, F. (1992) Ca^{2+}/calmodulin-regulated nitric oxide synthases. *Cell Calcium*, **13**, 427–434.

45. Abbott, K.L., Friday, B.B., Thaloor, D., Murphy, T.J. and Pavlath, G.K. (1998) Activation and cellular localization of the cyclosporine A-sensitive transcription factor NF-AT in skeletal muscle cells. *Mol. Biol. Cell.*, **9**, 2905–2916.

46. Shen, T., Liu, Y., Randall, W.R. and Schneider, M.F. (2006) Parallel mechanisms for resting nucleo-cytoplasmic shuttling and activity dependent translocation provide dual control of transcriptional regulators HDAC and NFAT in skeletal muscle fiber type plasticity. *J. Muscle Res. Cell. Motil.*, **27**, 405–411.

of passive calcium leak from the SR. *Am. J. Physiol. Cell. Physiol.*, **292**, C1591–C1598.

47. Allen, D.L., Uyenishi, J.J., Cleary, A.S., Mehan, R.S., Lindsay, S.F. and Reed, J.M. (2010) Calcineurin activates interleukin-6 transcription in mouse skeletal muscle *in vivo* and in C2C12 myotubes *in vitro*. *Am. J. Physiol. Regul. Integr. Comp. Physiol.*, **298**, R198–R210.

48. Nilsson, L.M., Sun, Z.W., Nilsson, J., Nordström, I., Chen, Y.W., Molkentin, J.D., Wide-Swensson, D., Hellstrand, P., Lydrup, M.L. and Gomez, M.F. (2007) Novel blocker of NFAT activation inhibits IL-6 production in human myometrial arteries and reduces vascular smooth muscle cell proliferation. *Am. J. Cell. Physiol.*, **292**, C1167–C1178.

49. Tsujinaka, T., Fujita, J., Ebisui, C., Yano, M., Kominami, E., Suzuki, K., Tanaka, K., Katsume, A., Ohsugi, Y., Shiozaki, H. and Monden, M. (1996) Interleukin 6 receptor antibody inhibits muscle atrophy and modulates proteolytic systems in interleukin 6 transgenic mice. *J. Clin. Invest.*, **97**, 244–249.

50. Ebisui, C., Tsujinaka, T., Morimoto, T., Kan, K., Iijima, S., Yano, M., Kominami, E., Tanaka, K. and Monden, M. (1995) Interleukin-6 induces proteolysis by activating intracellular proteases (cathepsins B and L, proteasome) in C2C12 myotubes. *Clin. Sci. (Lond.).*, **89**, 431–439.

51. Levano, S., Vukcevic, M., Singer, M., Matter, A., Treves, S., Urwyler, A. and Girard, T. (2009) Increasing the number of diagnostic mutations in malignant hyperthermia. *Hum. Mutat.*, **30**, 590–598.

52. Treves, S., Vukcevic, M., Griesser, J., Franzini-Armstrong, C., Zhu, M.X. and Zorzato, F. (2010) Agonist activated calcium influx occurs at stable plasmalemma-endoplasmic reticulum junctions. *J. Cell Sci.*, **123**, 4170–4181.